

**Key Points:**

- Exploring the Indian Ocean sea temperature errors
- Identifying the initial errors that frequently cause spring predictability barrier for Pacific El Niño
- Exploring the evolutionary mechanism of such errors and its implication to El Niño predictions

Correspondence to:

W. Duan,
duanws@lasg.iap.ac.cn

Citation:

Zhou, Q., Mu, M., & Duan, W. (2019). The initial condition errors occurring in the Indian Ocean temperature that cause “spring predictability barrier” for El Niño in the Pacific Ocean. *Journal of Geophysical Research: Oceans*, 124. <https://doi.org/10.1029/2018JC014403>

Received 29 JUL 2018

Accepted 27 JAN 2019

Accepted article online 30 JAN 2019

The Initial Condition Errors Occurring in the Indian Ocean Temperature That Cause “Spring Predictability Barrier” for El Niño in the Pacific Ocean

Qian Zhou^{1,2}, Mu Mu³ , and Wansuo Duan^{2,4} 

¹National Marine Environmental Forecasting Center, Beijing, China, ²LASG, Institute of Atmospheric Physics, Chinese Academy of Sciences, Beijing, China, ³Institute of Atmospheric Sciences, Fudan University, Shanghai, China, ⁴University of Chinese Academy of Sciences, Beijing, China

Abstract The Community Earth System Model is used to explore the influences of the initial condition errors in sea temperatures in the Indian Ocean (related initial condition errors) on the uncertainties in the Pacific El Niño predictions. Two categories of Indian Ocean-related initial condition errors are shown to frequently induce the “spring predictability barrier” for El Niño events. The category-1 error consists of a positive Indian Ocean Dipole-like sea temperature pattern over the Indian Ocean while the category-2 initial condition error has a negative Indian Ocean Dipole-like sea temperature structure and is nearly opposite to that of the category-1. Both categories of errors underestimate the Pacific El Niño in terms of its amplitude, although they present different spatial structures and undergo different mechanisms. Specifically, the category-1 error induces negative errors in El Niño predictions in terms of its amplitude by tropical oceanic channel Indonesian Throughflow while the category-2 error exerts its impact on El Niño prediction and makes it underestimate through the atmospheric bridge. Both categories of initial condition errors emphasize the sensitivity of El Niño predictions to the initial uncertainties in sea temperatures in the Indian Ocean. They may therefore provide useful information on how initialization in the Indian Ocean can be utilized to improve El Niño predictions.

Plain Language Summary The skill of the El Niño predictions often decline dramatically when the predictions bestride the boreal spring. This phenomenon is “spring predictability barrier” for El Niño predictions. Considering the interaction between tropical Pacific and Indian Ocean, the present study explores the role of the sea temperature errors in the tropical Indian Ocean in generating spring predictability barrier of Pacific El Niño and identifies two types of initial errors that frequently cause significant spring predictability barrier. These two types of errors emphasize the mechanism of atmosphere bridge and oceanic channel in connecting tropical Indian Ocean and Pacific Ocean, respectively. They also provide useful information on how initialization of numerical model can be utilized to improve the El Niño predictions.

1. Introduction

The climate mode of El Niño–Southern Oscillation (ENSO) is of the strongest interannual variability, which occurs in the tropical Pacific and often brings about extreme weather and climate events over the world (Alexander et al., 2002; Henderson et al., 2018; Wang et al., 2000). It is therefore aggressively important to improve the level of ENSO prediction skills (Kirtman et al., 2002; Zhu et al., 2013).

Great progresses have been achieved to the ENSO either in theories or in predictions (Tang et al., 2018), but so far the ENSO predictions are not of satisfied skill and large uncertainties exist in realistic forecasts (Kumar et al., 2017; Tippett et al., 2011). Particularly, when predictions are performed across the spring, the anomaly correlation skill of ENSO predictions is inclined to decline dramatically. This low skill in predictions for ENSO is often called “spring predictability barrier” (SPB) phenomenon (Lai et al., 2018; Larson & Kirtman, 2016; Webster & Yang, 1992; Zhang et al., 2005). In terms of error growth, a notable SPB is related to the predictions that are of large errors at the given lead time and whose error growth rates are the largest in the boreal spring (Yu et al., 2009).

The effect on the SPBs of initial condition errors was investigated by optimal initial perturbation approaches (Moore & Kleeman, 1996; Mu, Duan, et al., 2007; Mu, Xu, et al., 2007). Then an initial condition error of explicit structure was identified and confirmed to be more possible to result in SPB in an intermediate model (Mu, Xu, & Duan, 2007). Duan and Wei (2013) recognized such initial condition error mode in realistic predictions of ENSO. Therefore, the argument is that ENSO forecast skills could be significantly enhanced when the initial condition error mode associated with SPB is eliminated from the initial fields of the ENSO realistic predictions. Particularly, Chen et al. (1995) reduced the effects of the SPB on ENSO prediction uncertainties by introducing the air-sea coupling in the initialization of the model of Zebiak and Cane (1987), which then increased the forecasting skill for ENSO, potentially indicating the correctness of this argument.

The results mentioned above mainly focus on how initial condition errors from tropical Pacific influence the predictability for ENSO (also see Zhang & Gao, 2016; Tao et al., 2018, 2017). As we know, although the ENSO event occurs in the tropical Pacific, it has very close connections with other oceans (Alexander et al., 2002; Latif & Barnett, 1995). Quite a few studies argued that the ENSO is often influenced by the Indian Oceanic sea surface temperature (SST) anomalies (Luo et al., 2010; Saji & Yamagata, 2003a). This indicates that the tropical Pacific ENSO forecast is influenced by the accuracy of initial states from the tropical Pacific Ocean, as well as that from the tropical Indian Ocean. That is, in ENSO forecasting, we should consider the effects of initial condition uncertainties from both the tropical Pacific and Indian Oceans to potentially further improve the ENSO prediction skill. Actually, it has been suggested that ENSO predictions generated by either statistical or dynamical models can be improved if the Indian Ocean information is included (Luo et al., 2010). Particularly, Izumo et al. (2010) improved the forecasting skills of ENSO by adopting the Indian Dipole Mode Index in boreal autumn and its related tropical Pacific warm water volume as the leading predictors of the El Niño peak (also see Izumo et al., 2014). It is therefore implied that the prediction skills of ENSO events are also significantly influenced by the uncertainties originated from the tropical Indian Ocean.

The atmospheric bridge connecting tropical Pacific to Indian Oceans has been suggested as a dominant way to the impact of the Indian Ocean on Pacific ENSO (Chen, 2011; Wu & Meng, 1998). The oceanic channel Indonesian Throughflow was also demonstrated to play important role in the positive Indian Ocean Dipole (IOD) forcing the Pacific ENSO events (Gordon, 2005; Tillinger & Gordon, 2009). Specifically, Yuan et al. (2011) showed that the positive IOD elevates the thermocline of the eastern Indian Ocean; then the elevated thermocline generates upwelling Kelvin waves that cross through the ITF and propagate into the eastern tropical Pacific Ocean, which then affect tropical Pacific ENSO. The negative IOD forcing is also shown to influence ENSO through the ITF (Zhou et al., 2015).

Is it the atmospheric bridge or the ITF that contributes to the mechanisms of the IOD that affect the ENSO-related sea surface temperature anomalies (SSTAs)? Obviously, the answer to this question remains controversial. In any case, it is true that the Indian Ocean SSTA for IOD can influence the Pacific SSTAs of ENSO and then the predictability of ENSO. Therefore, we ask the following: how does the Indian Ocean SSTA for IOD events exert influences on the ENSO predictability? Can the initial condition errors occurring in the Indian Ocean induce the SPB for ENSO predictions? What are the common features of the initial condition errors that frequently cause SPBs of ENSO? Additionally, how do these initial condition errors propagate to influence the ENSO predictability, via the atmospheric bridge or/and the ITF? The present paper attempts to address these questions.

In the following section, we will introduce the model and data adopted in the present study, and in section 3, we will describe the experimental strategy. Subsequently, in section 4 the initial errors over the Indian Ocean are shown to have possibilities to cause the SPB; and the initial errors making for a SPB are identified. Furthermore, their evolutionary mechanisms are also shown in this section, including an emphasis on the role of atmospheric bridge and ITF in Indian Ocean errors disturbing Pacific ENSO prediction uncertainties. In the last section, the paper provides a summary and a discussion.

2. The Climate Model and Its Validation

We adopt in the present study the Community Earth System Model (CESM1.0.3). The CESM1.0.3 is a coupled model, which was designed by the National Center for Atmospheric Research. It comprises

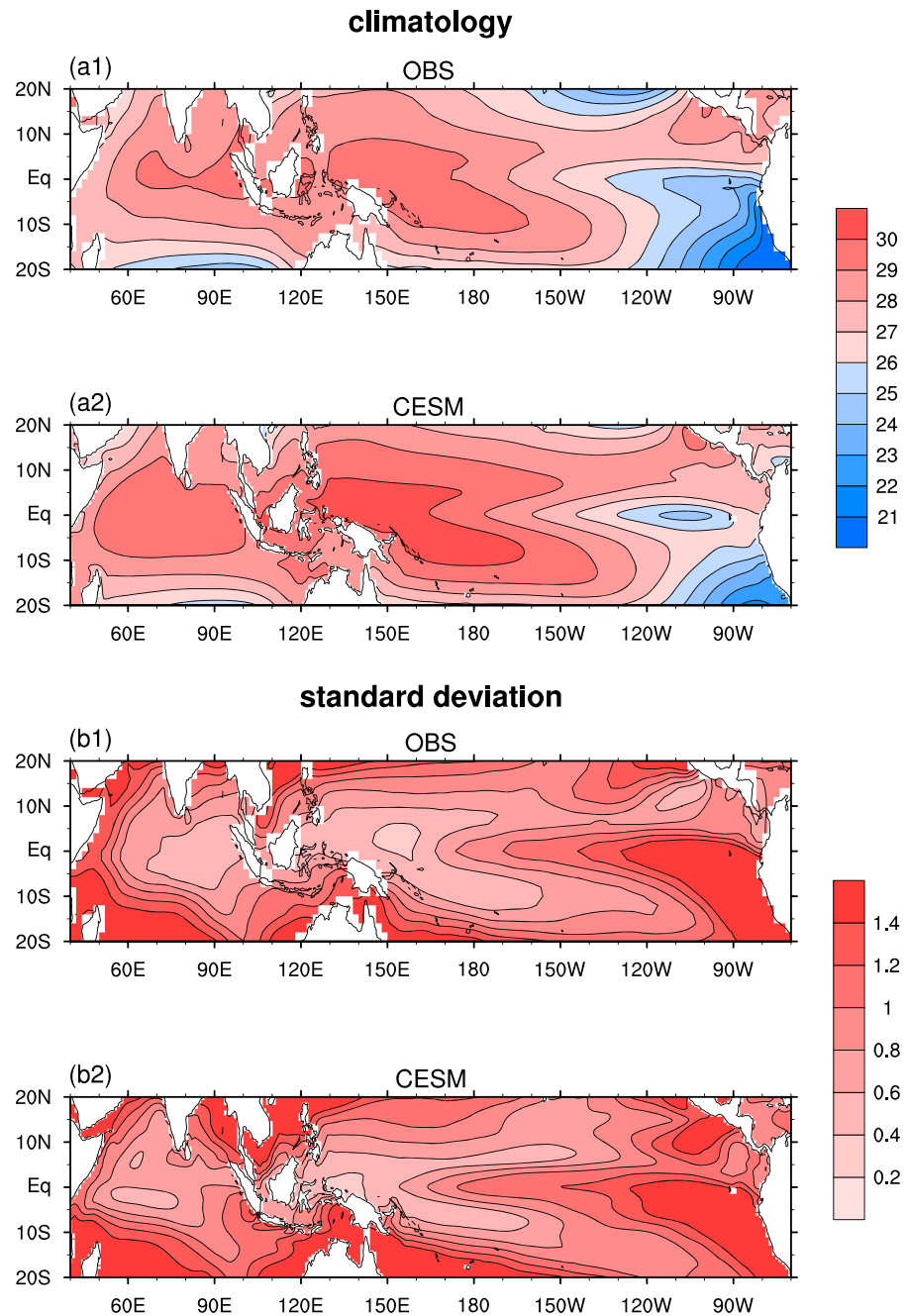


Figure 1. Climatology of SSTs ($^{\circ}\text{C}$) over the tropical Pacific and Indian Oceans derived from (a1) the monthly extended Reconstructed Sea surface temperature version 3 (ERSST V3) data set over the period 1961–2010 and (a2) CESM1.0.3; the standard deviation of the SSTs in the tropical oceans derived from (b1) the monthly extended Reconstructed Sea surface temperature version 3 (ERSST V3) data set for the period 1961–2010 and (b2) CESM1.0.3.

multiple model components associated with atmosphere, land, ocean, and ice, and uses a flux coupler to couple them. The details of the CESM1.0.3 model's configuration can be found in Hurrell et al. (2013).

The CESM1.0.3 is numerically integrated for 150 model years with the external forcing being the year 2000's values for aerosols, tracer gases, land cover, and insolation. And only simulations of the model years from the 51st to the 150th (a total of 100 model years) are adopted. Based on this 100-year integration, in Figure 1, we plot the climatology and standard deviations of the SSTs in CESM1.0.3. Correspondingly, the climatology and standard deviation of the SSTs derived from observations are also plotted in Figure 1.

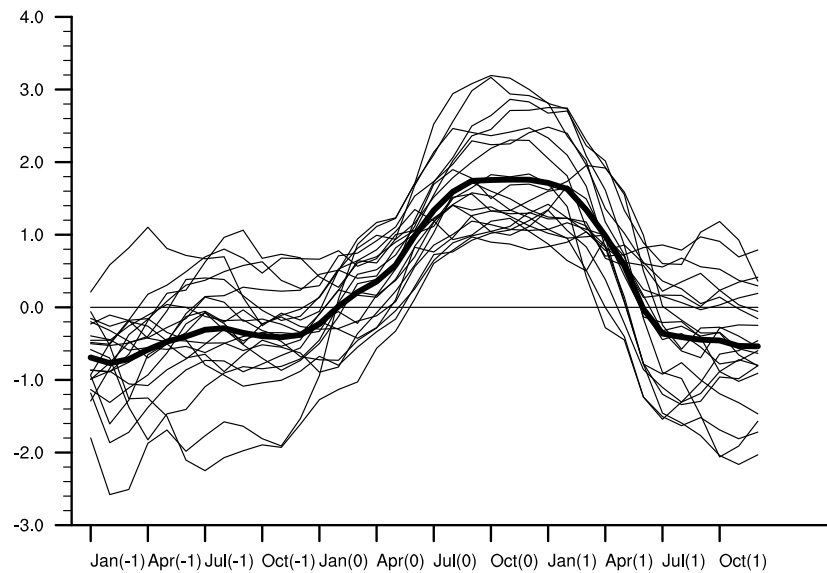


Figure 2. The Niño3 index of 20 El Niño events selected from CESM1.0.3. The thin lines represent all the 20 El Niño events and the thick line is the mean of the 20 events.

Figure 1a shows that the CESM1.0.3 produces an acceptable simulation of the climatological state of the SST component in either tropical Pacific or Indian Oceans, with slightly warmer SSTs in both tropical western Pacific and central Indian Oceans than those observed. The standard deviations of the SSTs in both oceans from CESM1.0.3 also agree with the observations, as shown in Figure 1b.

In addition to the climatological states of the tropical oceans, the most important air-sea interaction in each ocean is also well simulated. For the tropical Pacific, ENSO acts as the leading EOF mode in CESM1.0.3, and can explain 50.6% of the total variances of the anomalous SSTs during the D(0)J(1)F(1) season, where “D,” “J,” and “F” are short for December, January, and February and “0” and “1” signify the El Niño year and the next year, respectively. This feature is very similar to the observations, which present ENSO as the dominant EOF mode responsible for explaining 55.3% of the variances. The power spectrum of the related Niño3 index from CESM1.0.3 shows a period of three to six years for ENSO, which is also in accordance with the observations. Figure 2 shows 20 typical El Niño events simulated from this model. Obviously, the El Niño events from this model usually start warming in January (0), reach the peak at the end of the year, and then decay afterward, indicating an acceptable simulation of the phase-locked feature. The IOD events occurring in the Indian Ocean are also well simulated. Considering that the observed IOD events usually peak in the autumn, we perform an EOF analysis to the SSTA during the period of September-October-November. As a result, a dipole mode with positive and negative SSTA, respectively, in the western and eastern Indian Oceans is presented as the dominant EOF mode responsible for 25.8% of the total variances of the observations. The IOD pattern also leads as the first EOF in CESM1.0.3, but explains 63.9% of the total variance. This deficiency of the simulation might be caused by the fixed forcing applied to the coupled model without the global warming trend. The Dipole Mode Index, followed the definition of Saji et al. (1999), is also obtained by subtracting SST averaged over the western Indian Ocean from that over the eastern Indian Ocean. By analyzing the power spectrum, the Dipole Mode Index derived from the CESM1.0.3 is found to have a period of one to two years for IOD events.

Since the IOD occurring in the Indian Ocean can affect the ENSO through the atmospheric bridge or the ITF, their simulations in this coupled model are also evaluated. The rising branch of the climatological tropical atmospheric bridge in this model is located over the region of eastern Indian Ocean and western Pacific Ocean; while for the sinking branches, one is located over the tropical western Indian Ocean and the other is over the eastern Pacific Ocean. These basic features of the atmospheric bridge over the two tropical oceans agree with the observations. The ITF in the coupled model is also assessed. The ITF simulated in the CESM1.0.3 model is calculated along the IX01 line (i.e., the Fremantle-Sunda Straits, which connects the tropical Indian Oceans and Pacific Ocean) from the surface to 700-m depth in the Indonesian seas. As a result,

the averaged ITF reaches 10.7 Sv, with a significant seasonally dependent feature of the ITF showing peak in summer but decay in winter. The seasonally dependent feature is very similar to that observed (Shinoda et al., 2012). The CESM1.0.3 model can describe the role of atmospheric bridge and ITF in the IOD forcing disturbing the tropical Pacific SSTA. The analysis of the lag correlations of the model's long-term runs was completed following the example of Yuan et al. (2013). The IOD forcing in the CESM1.0.3 suggests that, just like in the observations, these systems can influence the ENSO-related SSTA in the Pacific through the ITF, but that the model overestimates the atmospheric bridge's role in the IOD forcing influencing the Pacific Ocean next year. For the role of the ITF, it was examined by closing the atmospheric bridge of the CESM1.0.3 (Zhou et al., 2015). For the positive IOD, it induces negative sea surface height anomalies in the eastern Indian Ocean, which then encourage local upwelling anomalies. These upwelling Kelvin anomalies go to the equatorial western Pacific Ocean and travel to the equatorial eastern Pacific, which finally make the SST there become cooling in the subsequent year. For the negative IOD, the influence is almost symmetric to that of the positive IOD events. These analyses indicate that the CESM1.0.3 can simulate the mechanisms responsible for positive and negative IOD disturbing ENSO-related SSTs in the subsequent year through the ITF.

In short, an acceptable simulation for both tropical Pacific and Indian Oceans can be provided by the CESM1.0.3; furthermore, either the atmospheric bridge or the ITF, which link these two tropical oceans, are also well simulated. It is therefore reasonable to use this coupled model to explore the influences of the initial condition errors originated over the tropical Indian Ocean on the prediction uncertainties of tropical Pacific El Niño and identify the roles that the ITF and atmospheric bridge played in the initial condition errors of the tropical Indian Ocean influencing El Niño predictions.

3. Experimental Design

Since the CESM1.0.3 can describe the essential features of the El Niño events observed in the reality and relevant interactions between tropical Pacific and Indian Oceans (see section 2), the El Niño events occurring in this coupled model can be regarded as “reference state” El Niño events to examine how the initial condition errors yield considerable forecast uncertainties. We select 20 model El Niño events (see Figure 2) from the 100-year integration of CESM1.0.3. Then we predict them for 12 months with the sea temperature field perturbed by the initial condition errors only over the tropical Indian Ocean. Here these initial condition errors are referred to as “IO-related initial condition errors.” Obviously, the forecast uncertainties herein are only caused by the IO-related initial condition errors and not contaminated by any model error (Qi et al., 2017). This strategy is similar to that in Shukla et al. (2017) and has been implemented by Feng et al. (2014) in an attempt to acquire the initial condition errors that considerably destroy the predictions of IOD events in the GFDL CM2p1 Coupled Model. Furthermore, Duan and Hu (2015) applied this strategy to the CESM1.0.3 and studied the initial condition errors that occurred in the Pacific Ocean and induced a notable SPB with respect to El Niño events.

The above strategy is similarly adopted in the present study to examine how IO-related initial condition errors exert effects on the El Niño predictions. Since the mature phase of the El Niño is often in winter, the forecasts for El Niño with the start months being October (−1) and January (0) and the lead time being 12 months will go through the spring season of the El Niño year, focusing on the predictions of El Niño onsets. Obviously, the spring season does not locate at the end of the forecast period, and therefore, even if the errors are large in spring, they will not be thought of as an accumulation of prediction errors, which is favorable for understanding the SPB associated with error growth. In the next section, we pay attention to such predictions and investigate how the IO-related initial condition errors affect the uncertainties associated with the SPB of concerned El Niño.

Numerical experiments are conducted for the selected 20 El Niño events to explore the IO-related initial condition errors frequently to yield a notable SPB. Specifically, a group of IO-related initial condition errors are chosen and superimposed on the El Niño and make idealized prediction experiments. Here the IO-related initial condition errors are obtained as follows. For the predetermined El Niño event, we subtract its Indian Ocean sea temperatures (40°E–130°E, 10°S–10°N; 0–400 m ranging from first to 30th levels of the ocean) at the start month from the corresponding monthly sea temperatures for every other month during the four years prior to the start month, then obtain some initial perturbations. For each start month, 24

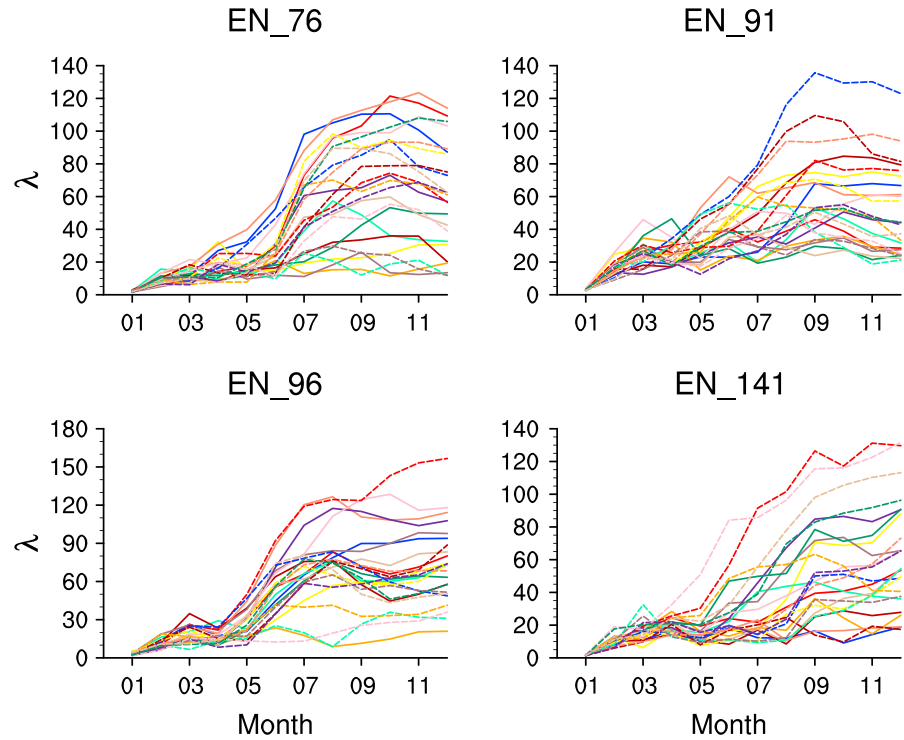


Figure 3. Examples of El Niño cases in terms of the evolutions of the prediction errors caused by the 24 IO-related initial condition errors with the start months of January (0), where the prediction errors are calculated according to $\lambda(t) = \|T^p(t) - T^r(t)\| = \sqrt{\sum_{ij} [T_{ij}^p(t) - T_{ij}^r(t)]^2}$ in section 4. “EN_*” denotes the model El Niño year and “*” describes the model year. Each of color lines represents the prediction error induced BY one IO-related initial condition error.

initial perturbations are obtained for one El Niño event and a total of 480 initial perturbations are then for predetermined 20 El Niño events. We can signify these initial perturbations as T' and makes $\|T'\| = \sqrt{\sum_{i,j,k} T'^2_{ijk}}$, where $T'_{i,j,k}$ denotes the values of T' at the spatial grid point (i,j,k) in the tropical Indian Ocean. Then we scale T' to T'_0 with $T'_0 = \frac{T'}{\|T'\|} \delta$, with $T'_0 = \{T'_{0i,j,k}\}$ and δ being the climatological variations of tropical Indian Ocean sea temperatures. We regard T_0 as the IO-related initial condition errors and a total of 480 IO-related initial condition errors are obtained. An EOF analysis is applied to these 480 IO-related initial condition errors, and the first 6 EOF modes are taken. With each of these EOF modes, the IO-related initial condition errors that have the highest positive and negative correlations with this EOF mode are selected, respectively. For the 6 EOF modes, 12 IO-related initial condition errors are obtained. Besides them, we randomly choose another 12 IO-related initial condition errors from the rest ones, which, together with the former 12 ones, comprise 24 IO-related initial condition errors for each start month. Then we superimpose these 24 IO-related initial condition errors on each El Niño event and integrate for 12 months from the different start months. Thus, for each start month, a total of 480 predictions are obtained with all the 20 El Niño events, where the prediction errors can be calculated by subtracting the reference state El Niño from its predictions. Clearly, these prediction errors are only resulted from the IO-related initial condition errors.

4. The SPB Phenomenon of El Niño Predictions

For the 24 IO-related initial condition errors obtained in section 3, we add them to each of the selected 20 El Niño events to be predicted and obtain perturbed initial conditions. With these perturbed initial conditions, we integrate the model for one year from the start months January (0) and October (-1), in attempt to predict the onsets of El Niño events. Here the resultant prediction errors for the SSTA component can be

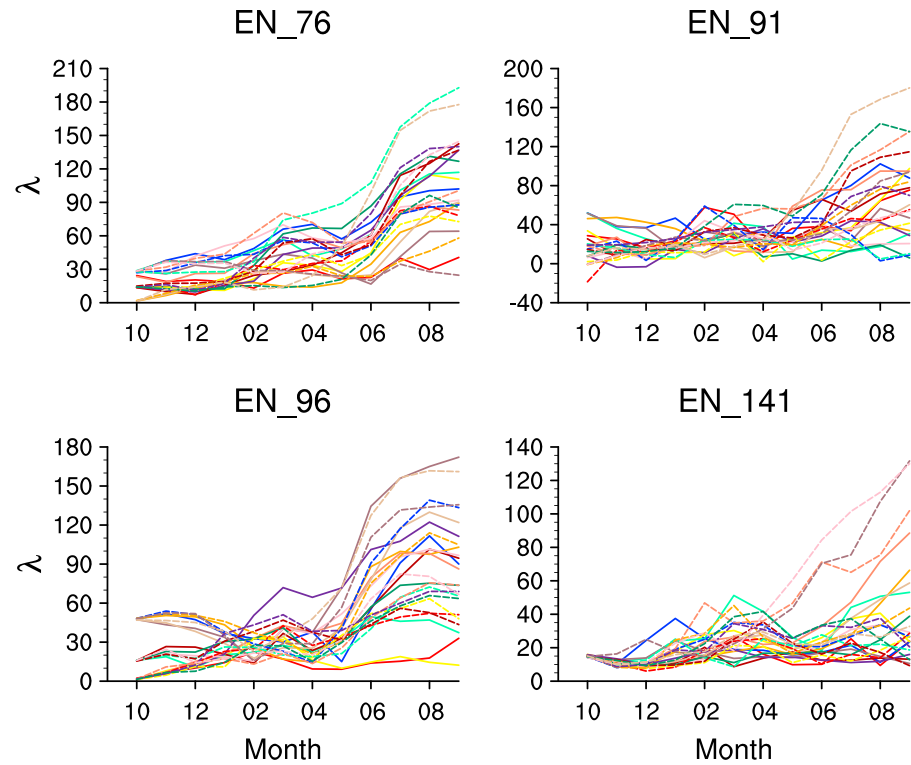


Figure 4. Same as in Figure 3 but for the El Niño predictions starting in October (−1).

obtained by estimating $\lambda(t) = \|T^p(t) - T^r(t)\| = \sqrt{\sum_{i,j} [T_{ij}^p(t) - T_{ij}^r(t)]^2}$, where λ is the prediction error and measured by the norm $\|\cdot\|$, T^p is the SSTA component of the predictions, T^r represents the SSTA of the El Niño event to be predicted, and the grid point (i, j) are those in the Niño3 region. To explore the SPB, a parameter γ is introduced to describe the season-dependent growth of prediction errors of El Niño, which can be calculated by $\gamma = \frac{\lambda(t_2) - \lambda(t_1)}{t_2 - t_1}$, where $\lambda(t_1)$ and $\lambda(t_2)$ are, respectively, the prediction errors at the initial time and final time of one season, and $t_2 - t_1$ measures the time length of the season. When γ is positive (negative), it corresponds to growth (decay) of prediction errors during the season. Furthermore, the larger absolute value of the γ implies the faster growth or decay of prediction errors. It is noted that the season of spring and the beginning summer is the time when quite a few models forecasts show SPB with respect to El Niño (Duan & Mu, 2018). Therefore, in the present study, if the prediction error of concerned El Niño events grows quickly during the season of spring and the beginning of summer and remains large values at the final time of the El Niño prediction, we think that an SPB occurs.

Through numerical experiments, it is found that the prediction errors for the selected 20 El Niño events are shown to grow sharply during June-July-August in some predictions and present large values at the end of the El Niño forecast period. This indicates that a quick drop in prediction skills occurs for these El Niño predictions during the spring and the beginning of summer, and makes the greatest contribution to the final prediction error for one-year lead time. Figures 3 and 4 show some examples of El Niño cases for their prediction error evolutions with the start months January (0) and October (−1), respectively. To clarify the characteristic for these El Niño predictions much more clearly, we select these predictions and plot the error growth rate for the predictions of the 20 El Niño and the related Niño3 index in Figure 5. It is shown that, such predictions, starting from either January (0) or October (−1), present larger final prediction errors and experience a quick error growth when the predictions go through the AMJ or JAS seasons (as shown in the histograms in Figure 5), indicating that significant SPBs occur. These predictions show that the IO-related initial condition errors are possible to result in significant SPBs. Furthermore, considering the one-year lead predictions initialized at the start months January (0) and October (−1), which bestrides the

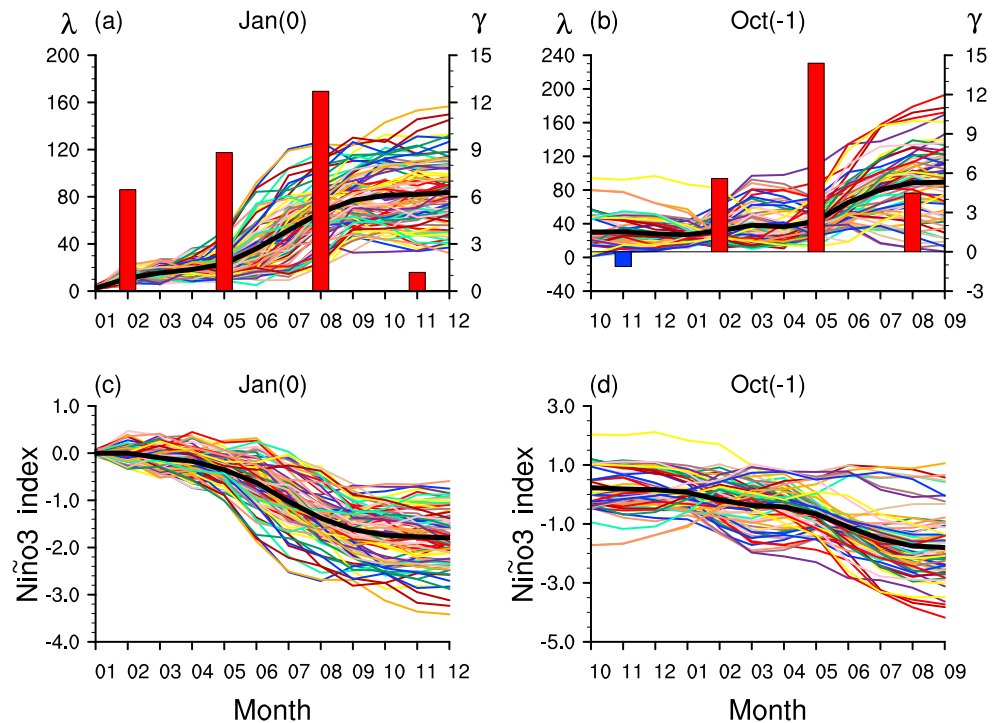


Figure 5. The means of the prediction errors caused by each SPB-related initial condition error (colored curves) for the 20 El Niño events with the start months of (a) January (0) and (b) October (−1), where the ensemble means of the seasonal growth rates of prediction errors are also plotted in histograms. (c and d) The corresponding Niño-3 index component (colored curves) of the prediction errors and their ensemble mean (thick black lines).

spring in the growth phase of El Niño, and that the spring is often the time of El Niño onset, the SPB is therefore thought to propose the challenge of forecasting the onset of El Niño. Besides, we note that the 24 IO-related initial condition errors often make the Niño3 indexes underestimated in term of their amplitudes, and the corresponding El Niño events false alarms.

As shown above, some predictions for El Niño show significant SPBs. However, which factors are responsible for the occurrence of SPB? Actually, in Figure 5, an SPB is shown to involve two uncertain factors: El Niño events themselves and initial condition errors. That is, some El Niño events are more possible to have an SPB while others are less so, but for an El Niño event, some initial condition errors result in an SPB more easily while others fail to do. Still, is it the El Niño events themselves or the initial condition errors that explain the occurrence of SPBs much more? Actually, the SPB has been clarified to be a result of the interaction among initial condition errors, El Niño itself, and related climatology (Mu, Duan, et al., 2007; Mu, Xu, et al., 2007). Despite thus, Duan and Hu (2015) used a complex general circulation model (GCM) and revealed the characteristics of the tropical Pacific sea temperature errors frequently to excite an SPB. In the present study, we attempt to explore what features the IO-related initial condition errors that frequently trigger a notable SPB with respect to El Niño. In order to do this, we select the El Niño events with favorable conditions for the occurrence of SPB.

By counting the number of the El Niño predictions with SPB, we find that, with the 24 IO-related initial condition errors disturbing, there are 12 El Niño events that tend to show more SPBs (details are omitted here) when the predictions start from January (0). This indicates that these 12 events are more likely to have SPBs under the effects of initial condition errors. To facilitate the description, we refer to these events as SPB-related El Niño events. However, we also find that, even though these events are more likely related to SPBs for the 24 IO-related initial condition errors, it is not all the initial condition errors that are likely to have the SPBs. As such, we naturally ask: what are the features of the SPB-related initial condition errors for 12 El Niño events with the start month January (0). Similarly, for predictions beginning from October (−1), we find out nine SPB-related El Niño events.

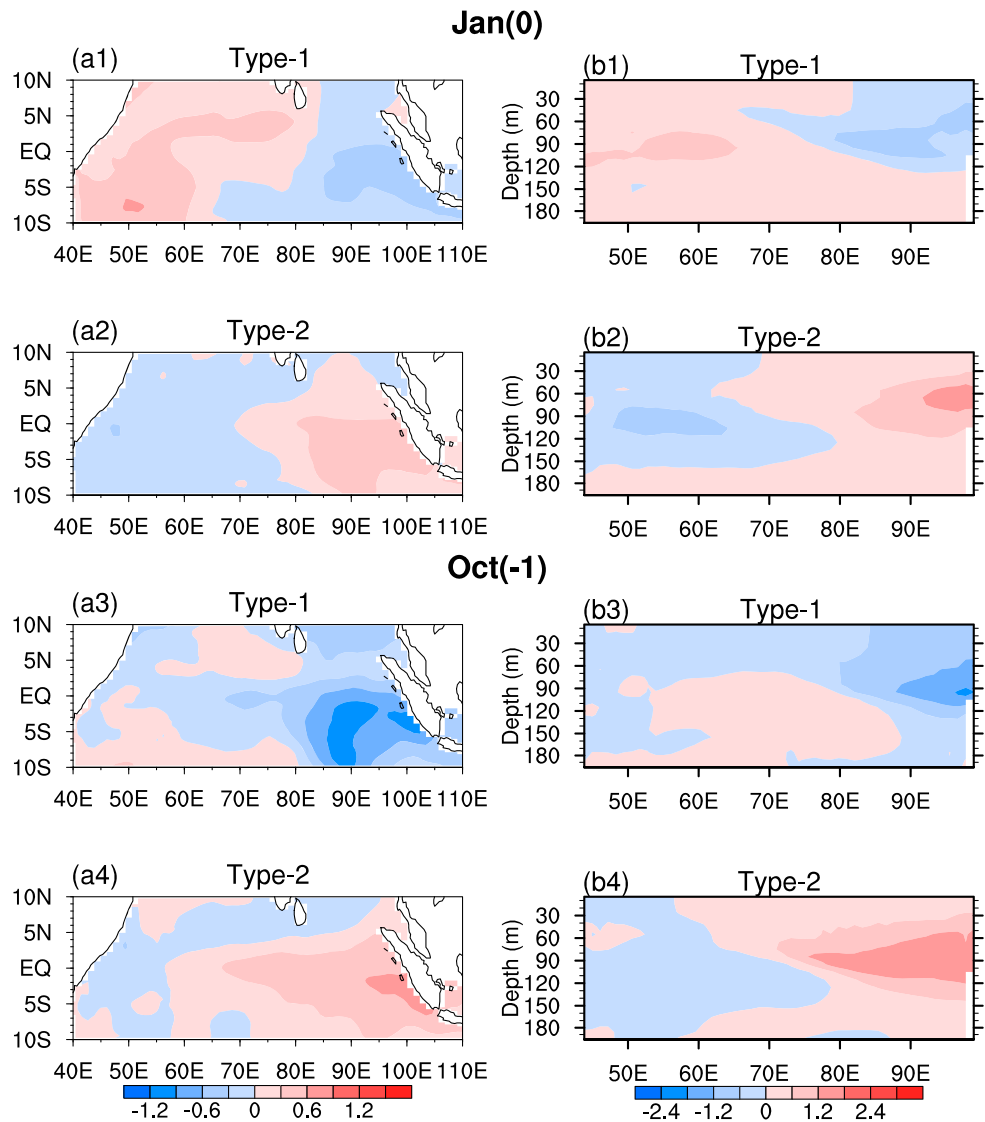


Figure 6. The SST and the vertical sea temperature (averaged by meridian 5°N to 5°S) components of the category-1 (a1 and b1) and category-2 (a2 and b2) SPB-related initial condition errors for January (0) as well as those of category-1 (a3 and b3) and category-2 (a4 and b4) SPB-related initial condition errors for October (−1).

4.1. The IO-Related Initial Condition Errors Frequently Causing an SPB

The 24 IO-related initial condition errors are commonly imposed on different El Niño events. For each IO-related initial condition error, we count the number of the resultant SPB-related El Niño events that show SPBs. In addition, with this number compared with those of other IO-related initial condition error, we can judge whether the IO-related initial condition error is the one that is more possible to yield a notable SPB. Actually, we select the IO-related initial condition errors at the start months of January (0) and October (−1) that cause more than half of the corresponding SPB-related El Niño events to show significant SPBs. These IO-related initial condition errors can be thought as being more possible to excite a considerable SPB and, for convenience, are entitled as “SPB-related initial condition errors.”

For the SPB-related initial condition errors, the spatial patterns are explored by using a cluster analysis approach with the measurements of the similarity coefficient. As a result, we find two categories of SPB-related initial condition errors for the start month January (0) (see Figure 6), which are labeled as category-1 and category-2 errors, respectively. By observing these patterns, we find that both categories of initial condition errors, on a large scale, are almost the same for the start month of January (0) as for the

start month October (−1), despite the differences in the details; nevertheless, the category-1 errors are almost opposite to the category-2 errors in signs. Specifically, the category-1 errors commonly present a positive IOD-like sea temperature pattern of dipole structure, with positive errors in the tropical western Indian Ocean but negative errors in the eastern Indian Ocean. Such a dipole mode is always much more significant at the subsurface than that at the surface. However, the category-2 errors show a negative IOD-like sea temperature structure which exhibits signs opposite to the category-1 errors.

4.2. Evolutionary Mechanisms of SPB-Related Initial Condition Error

Mu, Duan, et al. (2007) focused on the initial condition errors originated from the tropical Pacific and explained the SPB with respect to El Niño events. They clarified that the SPB can result from the spring's fastest-growing prediction errors that occurred in the tropical Pacific Ocean, which were shown to be caused by the climatological spring's strongest air-sea coupling instability in the tropical Pacific (Mu, Duan, et al., 2007; Mu, Xu, et al., 2007). In the last section, we have shown that the uncertainties occurring in the SST of the Indian Ocean can also cause large prediction errors for the tropical Pacific El Niño and induce its notable SPBs. Now we use the explanation of Mu, Duan, et al. (2007) to the SPB to explore the mechanism responsible for the evolution of the SPB-related initial condition errors originated from the tropical Indian Ocean. It is conceivable that the two factors of climatology and El Niño events responsible for the SPB in the Mu, Duan, et al. (2007)'s explanation are also robust for the seasonal evolutions of the SPB-related initial condition errors in the tropical Indian Ocean. Therefore, to explain the SPB induced by the initial condition errors originated from tropical Indian Oceans, we only need to explore how the two categories of SPB-related initial condition errors arising from the tropical Indian Ocean propagate to the tropical Pacific and influence El Niño prediction uncertainties.

As mentioned in section 1, the IOD can influence the tropical Pacific SST for ENSO via the ITF (Yuan et al., 2011, 2013; Zhou et al., 2015). There also exist some studies that emphasized the role of atmospheric bridge connecting the tropical Pacific to the Indian Oceans. In fact, a Gear-like coupling between the Indian and Pacific oceans (GIP) has been known as one of the popular atmospheric bridge theories for interpreting the interactions between the air-sea coupling system over tropical Indian and that over the Pacific Ocean (Wu & Meng, 1998). A positive rotating GIP consists of a clockwise Walker circulation anomaly and a counterclockwise monsoon anomaly over the tropical Indian Ocean. The positive GIP is often accompanied by a La Niña-like event. The mechanism of the GIP indicates that the air-sea interactions in one ocean basin can cause those in the other ocean due to zonal wind stress anomalies, then causing SST anomalies there. Meng and Wu (2000) verified that the monsoonal zonal flow anomaly over the tropical Indian Ocean can affect the air-sea coupling over the central and eastern Pacific Ocean via GIP and can trigger the onset of the tropical Pacific ENSO events. In fact, IOD events also occur with anomalous equatorial zonal wind, which bears similarities with the anomalous monsoon wind over the equatorial Indian Ocean (Saji & Yamagata, 2003b), so the mechanism of GIP also works to explain the atmospheric connections between the IOD and ENSO. Therefore, to explain the mechanism of the two categories of SPB-related initial condition errors influencing tropical Pacific El Niño prediction uncertainties, we should especially clarify the roles of the atmospheric bridge and ITF during the error evolutions.

For the El Niño forecasts in section 3, we find that, for every initial condition error in category-1 and category-2 errors, the evolutionary behaviors are similar. Furthermore, for the start month of either January (0) or October (−1), the category-1 and category-2 errors tend to have similar evolutionary mechanisms. Therefore, for simplicity, the evolutions of the prediction errors induced by the category-1 and category-2 errors are subsequently explored by composite analysis approach. Furthermore, only those with the start month of January (0) are used as examples to describe the results. The composites of the evolutions of the category-1 and category-2 errors are, respectively, plotted in Figures 7 and 8, where the sea temperature component over the vertical tropical oceans (averaged from 5°N to 5°S) is presented and the statistically significant values (>95%) are shown in dots. It is shown that the category-1 errors initially behave with a positive IOD-like decaying mode in the tropical Indian Ocean and then reverse to be a negative IOD-like evolving mode that peaks in December of the El Niño year. Correspondingly, the errors present initially negative anomalies of sea temperature in the tropical western Pacific, then propagate eastward, and finally form a tropical Pacific La Niña-like mode, making the El Niño amplitude underestimated and allowing a false alarm to the onset of El Niño. To find the connection between the SPB-related initial condition error

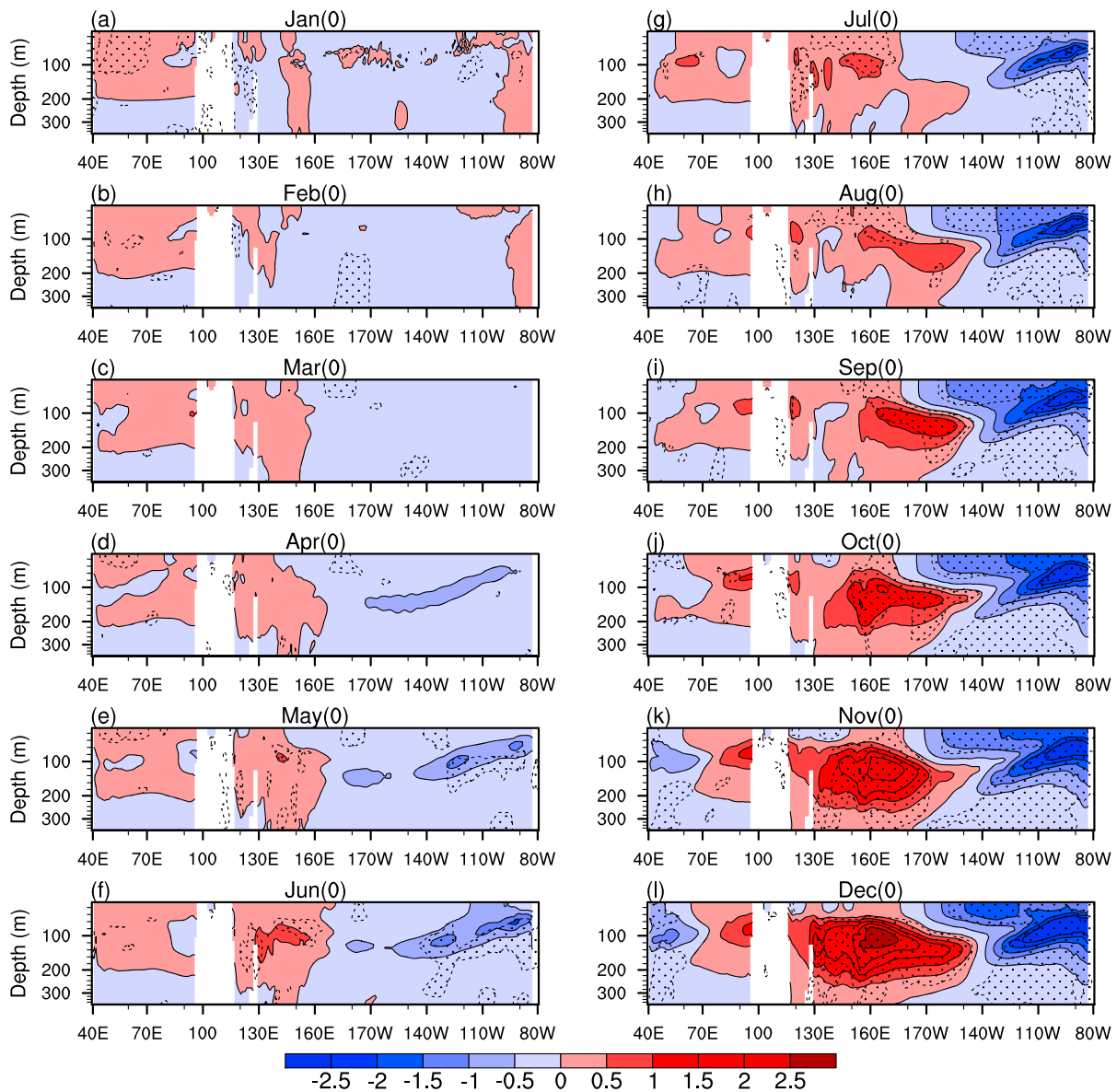


Figure 7. The composite monthly sea temperature component (averaged meridional over 5°N to 5°S) for the evolutions of the category-1 errors with the start month of January (0); the regions covered by dots indicates those of statistical significance (>95%).

and its resulting prediction error in the Pacific, in Figure 9, we randomly take one El Niño event as example and plot the first-four-month evolutions of the errors caused by the category-1 errors, with the components of SST, sea surface height, and vertical sea temperature averaged over meridional 5°N to 5°S. It can be seen from Figure 9 that the negative error of the sea temperature in the tropical eastern Indian Ocean tend to induce negative sea surface height and indicate an upwelling occurred in this region. Then, the upwelling Kelvin wave propagates to the tropical western Pacific and results in negative error of the SST in the tropical western Pacific. These negative SST errors continue to go into the tropical eastern Pacific due to the interactions of the ocean and atmosphere and present a La Niña-like evolving mode of prediction errors caused by the category-1 errors. Since the ITF and atmospheric bridge are two possible ways that connect the tropical Indian Ocean to the Pacific Ocean, then, is it ITF or atmospheric bridge that makes greater contributions to the propagation of prediction errors?

To examine whether the ITF contributes to the propagation of prediction errors caused by the category-1 errors to Pacific Ocean, we calculate the ITF volume transport component corresponding to the

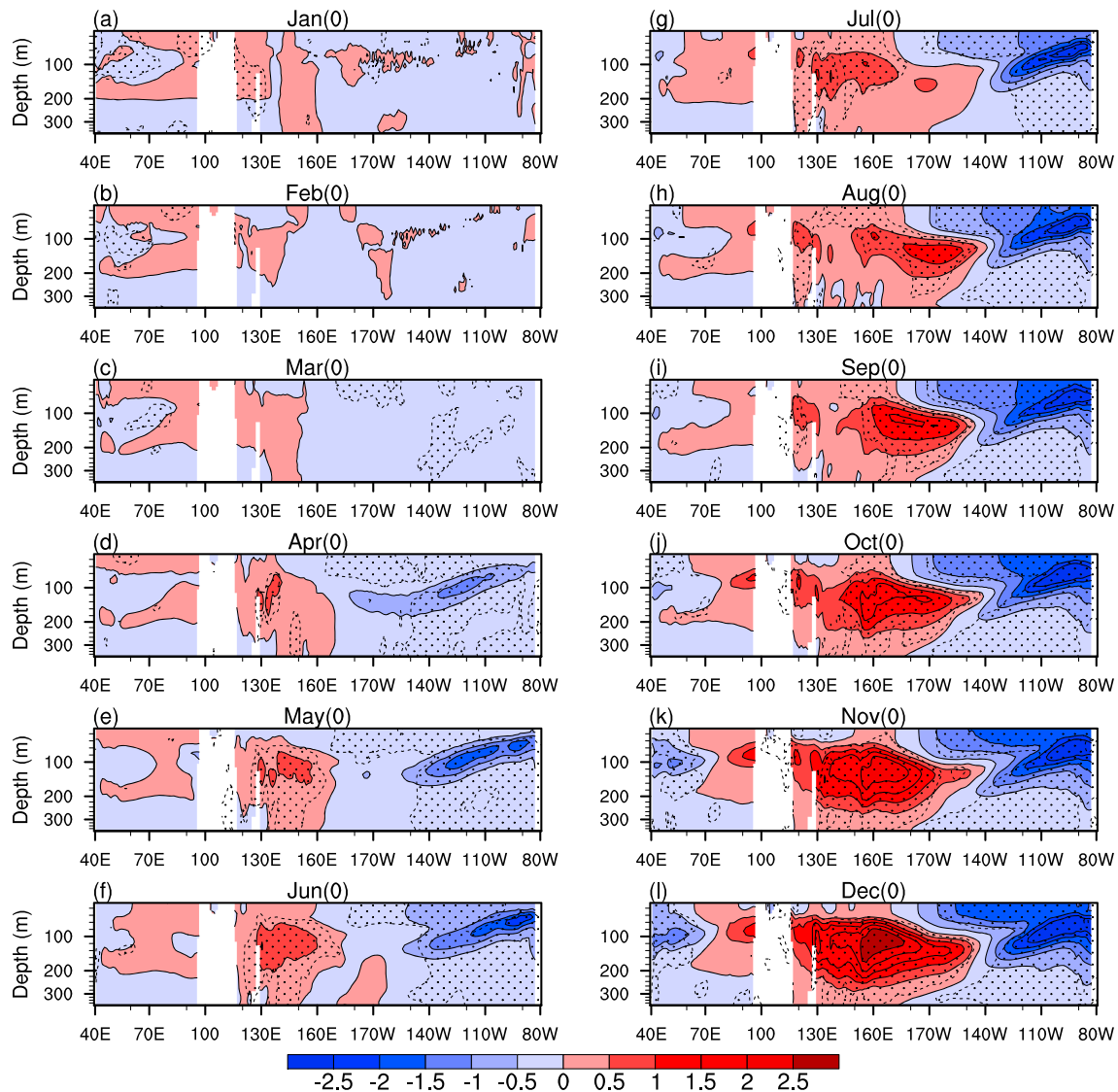


Figure 8. Same as in Figure 7 but for the category-2 errors with the start month of January (0).

prediction errors, showing that the averaged ITF during the first-four-month evolution of prediction errors can reach 0.85 Sv. The positive ITF indicates that the western Pacific warm pool loses more warm water volume to the Indian Ocean (Zhou et al., 2015), which can also be understood as that the anomalously cooling water in the eastern Indian Ocean penetrates into the tropical western Pacific. Thus, the value of 0.85 Sv during the evolution of the category-1 errors indicates that the negative error of the sea temperature in the eastern Indian Ocean propagates to the Pacific Ocean and causes negative SST errors occurring in the tropical western Pacific (see Figure 9), where the ITF plays the role in connecting the Indian Ocean to the Pacific Ocean. So the ITF makes contribution to the propagation of the category-1 errors from the Indian Ocean to the Pacific Ocean. For the atmospheric bridge, if it dominates in the process of SPB-related errors disturbing the predictions of El Niño events, an anomalous easterly wind over the tropical Indian Ocean can be caused by the category-1 errors in terms of their positive IOD-like mode. Through the connection of GIP (Wu & Meng, 1998), an anomalous westerly wind will emerge over the tropical Pacific, which can result in anomalous warm temperatures in the tropical eastern Pacific and cause El Niño to be overestimated in terms of its amplitude. However, as seen from Figure 7, the influence of the category-1 errors results in negative errors of the sea temperature in the tropical Pacific. Therefore, it is the oceanic channel ITF

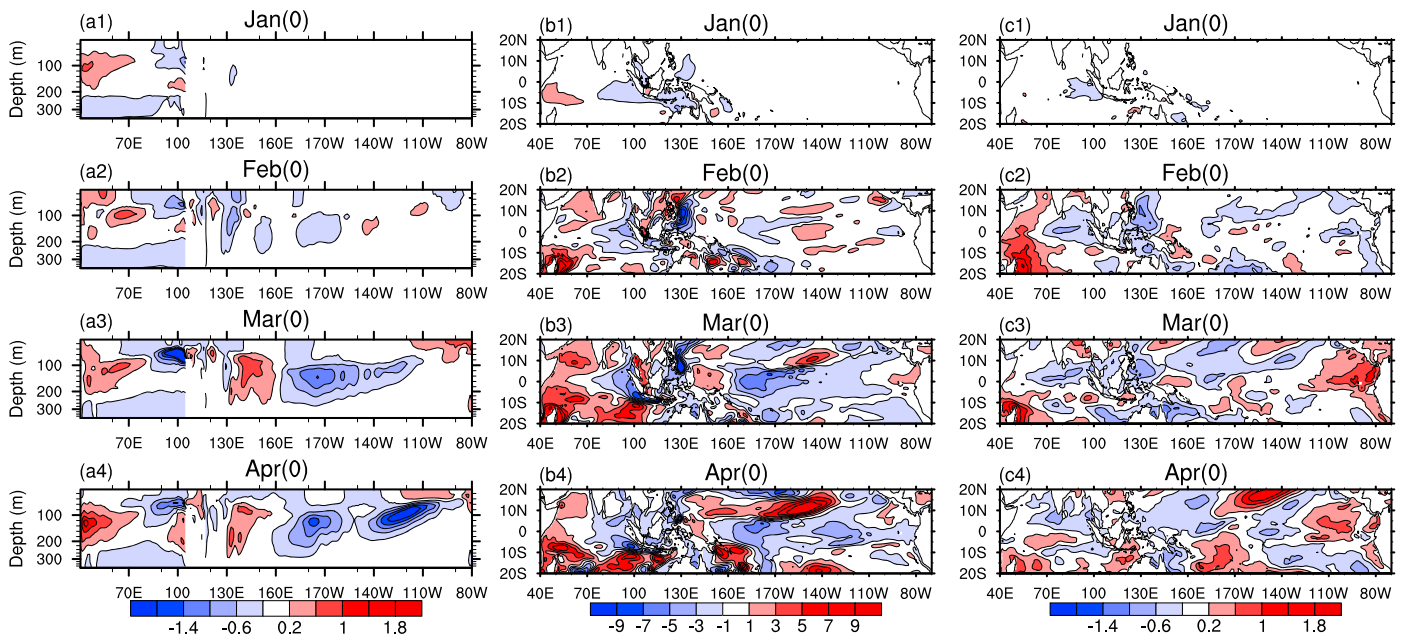


Figure 9. Evolution of the category-1 error from January (0) to April (0) with the components of (a) the vertical sea temperature in tropical Indian Ocean and Pacific Ocean over equator, (b) the SSH errors, and (c) the SST errors. The related El Niño event here, as an example, is the model El Niño event EN_141.

rather than the atmospheric bridge that plays the dominant role in the SPB-related category-1 errors influencing the ENSO-related SSTA prediction uncertainties.

In terms of the category-2 errors, their resultant prediction errors are of different evolutionary behaviors. As shown in Figure 8, the category-2 errors tend to present in the tropical Indian Ocean a negative IOD-like evolving mode with the peak in December of the El Niño year and show negative sea temperature errors mainly in the tropical eastern Pacific, as seen in the category-1 errors. These errors keep evolving locally and maintain a La Niña-like evolutionary mode, finally causing the underestimation of El Niño in terms of its amplitude. The mechanism that connects the Indian Ocean to Pacific Ocean under the influences of the category-2 errors follows. When the category-2 errors are superimposed on the tropical Indian Ocean, they will cause positive errors of the sea temperature in the tropical eastern Indian Ocean. If the category-2 errors influence the tropical Pacific via the ITF, these positive errors will induce positive errors of the sea temperature over the tropical western Pacific. Then, the anomalous ITF should be negative. However, when we compute the averaged anomalous ITF during the first-four-month evolution of the prediction errors induced by the category-2 errors, the averaged anomalous ITF is found to be 0.68 Sv. Hence, the category-2 errors are not mainly propagated through the ITF to influence the El Niño in the Pacific. Instead, it may be the atmospheric bridge that plays the role in the influence of the category-2 errors on the Pacific El Niño prediction uncertainties. In fact, the category-2 errors present positive errors in the sea temperature in the tropical eastern Indian Ocean, which induce anomalously westerly winds over the central tropical Indian Ocean (see Figure 10). These anomalously westerly wind cause anomalous updrafts to occur over the tropical eastern Indian Ocean and, according to the GIP theory, simultaneously yield anomalous downdrafts and anomalously easterly wind over the tropical Pacific Ocean. Exactly, the downdrafts appear over the tropical central-eastern Pacific (see Figure 11b), which, together with the anomalously easterly wind along the equator, is favorable for the occurrence of La Niña-like errors. Therefore, for the category-2 errors, it is the atmospheric bridge rather than the ITF that dominates the process of the category-2 errors influencing the tropical Pacific El Niño prediction uncertainties.

From the above analysis, it is obvious that both categories of SPB-related errors make the Pacific El Niño underestimated but they possess different mechanisms responsible for their evolutions. For the category-1 errors, it is the ITF that plays a dominant role in SPB-related errors influencing the Pacific El Niño prediction uncertainties, while for the category-2 errors, the atmospheric bridge dominates the process of their effects

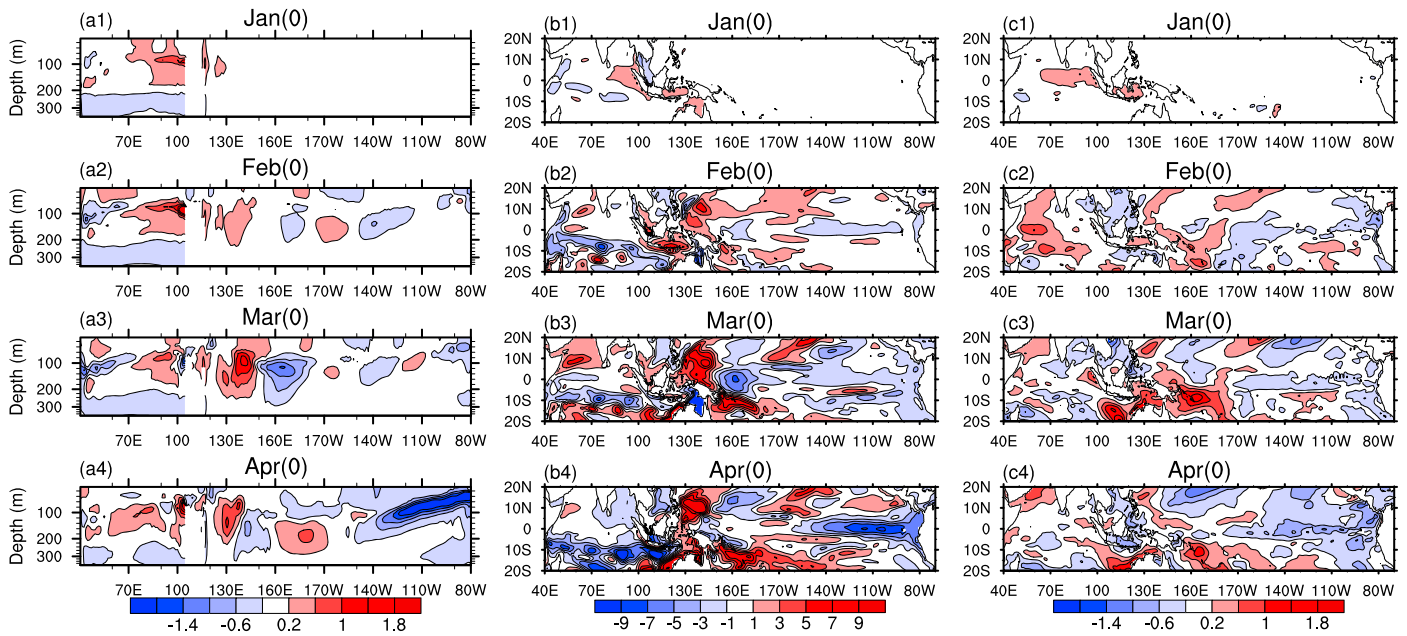


Figure 10. Same as in Figure 9 but for the evolution of the category-2 error and the model El Niño event EN_76.

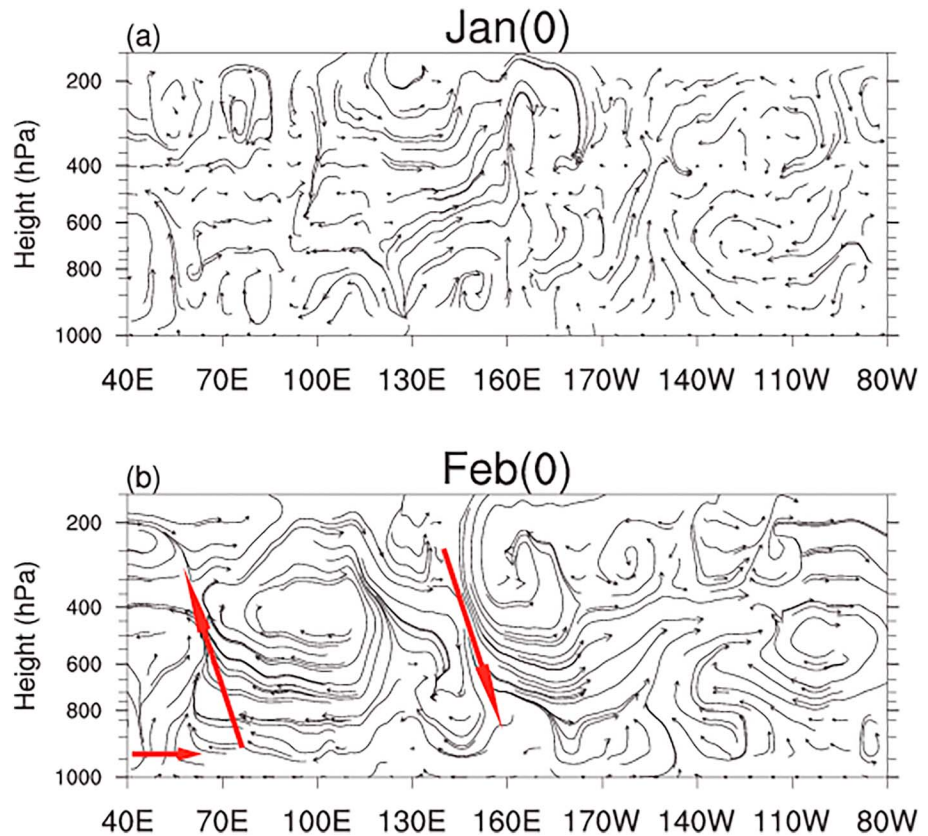


Figure 11. Evolutions of the category-2 error-induced wind errors, which are averaged meridional over 5°N to 5°S from the start month January (0) to February (0). The related El Niño is as in Figure 10.

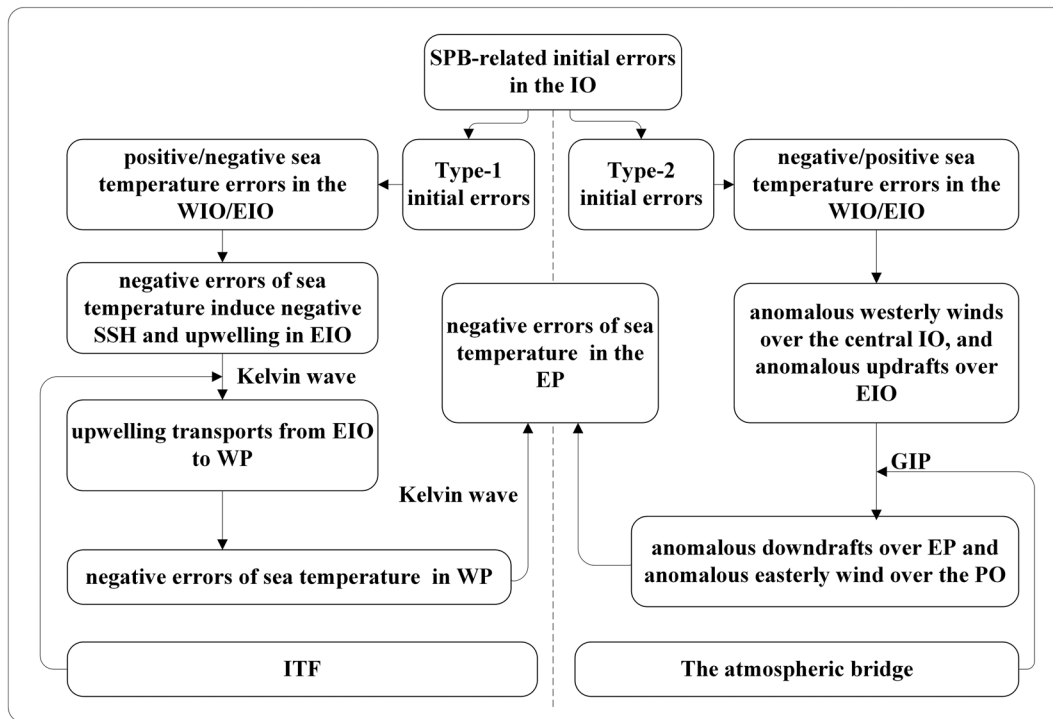


Figure 12. Schematic diagram for mechanisms of two categories of SPB-related initial condition errors in the Indian Ocean influencing the El Niño prediction uncertainties. “PO/IO,” “WP/EP,” and “WIO/EIO” are short for Pacific Ocean/Indian Ocean, western Pacific Ocean/eastern Pacific Ocean, and western Indian Ocean/eastern Indian Ocean, respectively.

on the Pacific El Niño prediction uncertainties. To make the mechanisms much clear, we summarize them in Figure 12.

5. Summary and Discussion

The present study explores whether or not the IO-related initial sea temperature errors can cause significant SPBs for El Niño predictions by using the coupled GCM CESM1.0.3. The results demonstrate that some IO-related initial condition errors cause significant SPBs but others induce a less significant SPB or fail to do so at all. Considering the severe effects of the SPB-related initial condition errors on El Niño forecast uncertainties, this study investigates their spatial structure characteristics. The results show that the SPB-related initial condition errors can be separated into two categories, that is, category-1 and category-2 initial condition errors. The former possess a pattern with positive errors on the sea temperature in the tropical western Indian Ocean and negative errors in the east, whereas the latter presents a spatial pattern nearly opposite to that of the category-1 in signs.

The category-1 errors develop with a positive IOD-like decaying mode in the initial period and then, in the latter period, reverse to show a negative IOD-like evolving mode in the tropical Indian Ocean; correspondingly, they exhibit negative errors on the sea temperature in the tropical western Pacific in the initial stage, which propagates eastward and then forms a La Niña-like error evolving mode, finally making the Pacific El Niño underestimated. By evaluating the atmospheric bridge and ITF, it is shown that the ITF can reach to 0.85 Sv during the evolution of the category-1 initial condition errors, which suggests that the anomalously negative sea temperatures that occur in the tropical western Pacific and finally make a La Niña-like mode in the tropical eastern Pacific can be gained from the anomalously negative sea temperature in the Indian Ocean by the ITF. For the atmospheric bridge, the category-1 errors induced anomalous easterly winds over the central Indian Ocean, which, by the GIP mechanism, can induce an anomalous westerly wind over the tropical Pacific and finally build up an El Niño-like mode, making the Pacific El Niño overpredicted. However, it is true that the category-1 errors cause the El Niño underestimated, which accords with the

role of the ITF (rather than the atmospheric bridge) in connecting the category-1 errors in the Indian Ocean to the tropical Pacific El Niño prediction uncertainties. Obviously, it is the ITF that plays a dominant role in the category-1 errors disturbing the Pacific El Niño forecast uncertainties. For the category-2 errors, they tend to induce a negative IOD-like evolving mode over the tropical Indian Ocean and present negative errors in the sea temperature in the tropical eastern Pacific. These negative errors are locally amplified and behave in a manner of La Niña-like evolving mode, causing the El Niño underestimated. Here the negative errors, which are induced by the category-2 errors, appear directly in the tropical eastern Pacific, which is not like the case of the category-1 errors propagating to the tropical western Pacific with negative sea temperature errors via the ITF. These explain that the atmospheric bridge plays a major role in the category-2 errors influencing the Pacific El Niño prediction errors.

It is noticed that both category-1 and category-2 errors present large sea temperature errors mainly in the subsurface of western and eastern Indian Ocean. Previous studies showed that, for the initial condition errors that exert larger influences on the prediction errors, the errors in the regions with large values often make greater contributions to prediction errors. Or say, the prediction errors are more sensitive to the initial condition errors in those regions. And the regions are often regarded as “sensitive areas” for targeting observations (Duan & Hu, 2015; Qin & Mu, 2012; Wang et al., 2013). When additional observations are increased in the sensitive areas and assimilated to the initial fields, the El Niño prediction skills can be improved much more than doing so in other areas. Then, whether or not the areas with large values of category-1 and category-2 errors represent the sensitive areas for the El Niño forecasting? Whether or not they are helpful for increasing the El Niño prediction skill? All these questions remain as scientific questions which should be addressed in future studies.

We should realize that the results obtained here are based on the model El Niño events, despite these El Niño events exhibit typical features of the observed ones. Therefore, one still needs to validate the results by more realistic prediction experiments. In this situation, one would explore how much the El Niño's forecast skill can be increased when the initial analysis is improved by filtering the component of SPB-related initial condition errors associated with model El Niño events. In addition, the experiments in the present study only care about the El Niño forecasts with the start months January (0) and October (−1) that bespide the development phase of El Niño events. In fact, attentions to the influences of the IO-related initial condition errors on the El Niño forecast bespiding its decaying phases should also be paid. Further, La Niña events also ought to be investigated to see how the IO-related initial condition errors affect their prediction errors. Then, the whole configuration of the IO-related initial condition errors influencing ENSO forecasts would be much clearer. In addition to the IO-related initial condition errors, the errors occurring in other ocean basins (like the Atlantic and North Pacific) are also of interests, especially caring about their effects on the predictability of ENSO events. It is believed that these studies would provide useful guidance for improving ENSO forecast skills.

Acknowledgments

The authors are grateful for the three anonymous reviewers for their insightful comments. This study was supported by the National Public Benefit (Meteorology) Research Foundation of China (grant GYHY201306018), together with the National Natural Science Foundation of China (grants 41525017, 41606031, 41690124, 41506040). The ERSST V3 data used here can be found at the website <https://www.ncdc.noaa.gov/data-access/marineocean-data/extended-reconstructed-sea-surface-temperature-ersst-v3b>. The data of tracer gases, insolation, aerosols, and land cover used in the CESM1.0.3 are from the website <https://svn-csm-inputdata.cgd.ucar.edu/trunk/inputdata/>. But the CESM1.0.3 model data and related codes are stored on the computers at State Key Laboratory of Numerical Modeling for Atmospheric Sciences and Geophysical Fluid Dynamics (LASG; <https://www.lasg.ac.cn>) and will be available to researchers upon request.

References

- Alexander, M., Blade, I., Newman, M., Lanzante, J., Lau, N. C., & Scott, J. D. (2002). The atmospheric bridge: The influence of ENSO teleconnections on air-sea interaction over the global oceans. *Journal of Climate*, *15*(16), 2205–2231. [https://doi.org/10.1175/1520-0442\(2002\)015<2205:tabtio>2.0.co;2](https://doi.org/10.1175/1520-0442(2002)015<2205:tabtio>2.0.co;2)
- Chen, D. (2011). Indo-Pacific Tripole: An intrinsic mode of tropical climate variability. *Advances in Geosciences*, *24*, 1–18. https://doi.org/10.1142/9789814355353_0001
- Chen, D., Zebiak, S. E., Busalacchi, A. J., & Cane, M. A. (1995). An improved procedure for El Niño forecasting: Implications for predictability. *Science*, *269*(5231), 1699–1702. <https://doi.org/10.1126/science.269.5231.1699>
- Duan, W. S., & Hu, J. Y. (2015). The initial condition errors that induce a significant “spring predictability barrier” for El Niño events and their implications for target observation: Results from an earth system model. *Climate Dynamics*, *1*, 376.
- Duan, W., & Wei, C. (2013). The “spring predictability barrier” for ENSO predictions and its possible mechanism: Results from a fully coupled model. *International Journal of Climatology*, *33*(5), 1280–1292. <https://doi.org/10.1002/joc.3513>
- Duan, W. S., & Mu, M. (2018). Predictability of El Niño–Southern Oscillation Events. *Oxford Research Encyclopedia of Climate Science*. <https://doi.org/10.1093/acrefore/9780190228620.013.80>
- Feng, R., Duan, W. S., & Mu, M. (2014). The “winter predictability barrier” for IOD events and its error growth dynamics: Results from a fully coupled GCM. *Journal of Geophysical Research: Oceans*, *119*, 8688–8708. <https://doi.org/10.1002/2014jc010473>
- Gordon, A. (2005). Oceanography of the Indonesian seas and their throughflow. *Oceanography*, *18*(4), 14–27. <https://doi.org/10.5670/oceanog.2005.01>
- Henderson, D. S., Kummerow, C. D., & Berg, W. (2018). ENSO influence on TRMM tropical oceanic precipitation characteristics and rain rates. *Journal of Climate*, *31*(10), 3979–3998. <https://doi.org/10.1175/jcli-d-17-0276.1>

- Hurrell, J. W., Holland, M. M., Gent, P. R., Ghan, S., Kay, J. E., Kushner, P. J., et al. (2013). The Community Earth System Model: A framework for collaborative research. *Bulletin of the American Meteorological Society*, *94*(9), 1339–1360. <https://doi.org/10.1175/BAMS-D-12-00121.1>
- Izumo, T., Lengaigne, M., Vialard, J., Luo, J. J., Yamagata, T., & Madec, G. (2014). Influence of Indian Ocean Dipole and Pacific recharge on following year's El Niño: Interdecadal robustness. *Climate Dynamics*, *42*(1-2), 291–310. <https://doi.org/10.1007/s00382-012-1628-1>
- Izumo, T., Vialard, J., Lengaigne, M., de Boyer Montegut, C., Behera, S. K., Luo, J. J., et al. (2010). Influence of the state of the Indian Ocean Dipole on the following year's El Niño. *Nature Geoscience*, *3*(3), 168–172. <https://doi.org/10.1038/ngeo760>
- Kirtman, B., Shukla, J., Balmaseda, M., Graham, N., Penland, C., Xue, Y., & Zebiak, S. (2002). Current Status of ENSO Forecast Skill a Report to the Climate Variability and Predictability (CLIVAR) Numerical Experimentation Group (NEG), CLIVAR Working Group on Seasonal to Interannual Prediction.
- Kumar, A., Hu, Z.-Z., Jha, B., & Peng, P. (2017). Estimating ENSO predictability based on multi-model hindcasts. *Climate Dynamics*, *48*(1-2), 39–51. <https://doi.org/10.1007/s00382-016-3060-4>
- Lai, A. W.-C., Herzog, M., & Graf, H.-F. (2018). ENSO forecasts near the spring predictability barrier and possible reasons for the recently reduced predictability. *Journal of Climate*, *31*(2), 815–838. <https://doi.org/10.1175/jcli-d-17-0180.1>
- Larson, S. P., & Kirtman, B. (2016). Drivers of coupled model ENSO error dynamics and the spring predictability barrier. *Climate Dynamics*, *48*(11-12), 3631–3644. <https://doi.org/10.1007/s00382-016-3290-5>
- Latif, M., & Barnett, T. P. (1995). Interactions of the tropical oceans. *Journal of Climate*, *8*, 952–964. [https://doi.org/10.1175/1520-0442\(1995\)008<0952:IOTTO>2.0.CO;2](https://doi.org/10.1175/1520-0442(1995)008<0952:IOTTO>2.0.CO;2)
- Luo, J. J., Zhang, R. C., Behera, S. K., Masumoto, Y., Jin, F.-F., Lukas, R., & Yamagata, T. (2010). Interaction between El Niño and extreme Indian Ocean Dipole. *Journal of Climate*, *23*(3), 726–742. <https://doi.org/10.1175/2009jcli3104.1>
- Meng, W., & Wu, G. X. (2000). Gearing between the Indo-Monsoon Circulation and the ENSO. Part II: Numerical Simulation (in Chinese). *Chinese Journal of Atmospheric Sciences*, *24*(1), 15–25. <https://doi.org/10.3878/j.issn.1006-9895.2000.01.02>
- Moore, A. M., & Kleeman, R. (1996). The dynamics of error growth and predictability in a coupled model of ENSO quarterly. *Journal of the Royal Meteorological Society*, *122*(534), 1405–1446. <https://doi.org/10.1002/qj.49712253409>
- Mu, M., Duan, W. S., & Wang, B. (2007). Season-dependent dynamics of nonlinear optimal error growth and El Niño-Southern Oscillation predictability in a theoretical model. *Journal of Geophysical Research*, *112*, D10113. <https://doi.org/10.1029/2005JD006981>
- Mu, M., Xu, H., & Duan, W. S. (2007). A kind of initial condition errors related to “spring predictability barrier” for El Niño events in Zebiak-Cane model. *Geophysical Research Letters*, *34*, L03709. <https://doi.org/10.1029/2006GL027412>
- Qi, Q. Q., Duan, W. S., Zheng, F., & Tang, Y. M. (2017). On the “spring predictability barrier” for strong El Niño events as derived from an intermediate coupled model ensemble prediction system. *Science China Earth Sciences*, *60*(9), 1614–1631. <https://doi.org/10.1007/s11430-017-9087-2>
- Qin, X. H., & Mu, M. (2012). Influence of conditional nonlinear optimal perturbations sensitivity on typhoon track forecasts quarterly. *Journal of the Royal Meteorological Society*, *138*(662), 185–197. <https://doi.org/10.1002/qj.902>
- Saji, N. H., Goswami, B. N., Vinayachandran, P. N., & Yamagata, T. (1999). A dipole mode in the tropical Indian Ocean. *Nature*, *401*(6751), 360–363. <https://doi.org/10.1038/43854>
- Saji, N. H., & Yamagata, T. (2003a). Possible impacts of Indian Ocean Dipole mode events on global climate. *Climate Research*, *25*, 151–169. <https://doi.org/10.3354/cr025151>
- Saji, N. H., & Yamagata, T. (2003b). Structure of SST and surface wind variability during Indian Ocean Dipole mode events: COADS observations. *Journal of Climate*, *16*(16), 2735–2751. [https://doi.org/10.1175/1520-0442\(2003\)016<2735:SOSASW>2.0.CO;2](https://doi.org/10.1175/1520-0442(2003)016<2735:SOSASW>2.0.CO;2)
- Shinoda, T., Han, W., Metzger, E. J., & Hurlburt, H. E. (2012). Seasonal variation of the Indonesian Throughflow in Makassar Strait. *Journal of Physical Oceanography*, *42*(7), 1099–1123. <https://doi.org/10.1175/jpo-d-11-0120.1>
- Shukla, R. P., Huang, B., Marx, L., Kinter, J. L., & Shin, C.-S. (2017). Predictability and prediction of Indian summer monsoon by CFSv2: Implication of the initial shock effect. *Climate Dynamics*, *50*(1-2), 159–178. <https://doi.org/10.1007/s00382-017-3594-0>
- Tang, Y. M., Zhang, R. H., Liu, T., Duan, W. S., Yang, D., Zheng, F., et al. (2018). Progress in ENSO prediction and predictability study. *National Science Review*, *5*(6), 826–839. <https://doi.org/10.1093/nsr/nwy105>
- Tao, L.-J., Gao, C., & Zhang, R. H. (2018). ENSO predictions in an intermediate coupled model influenced by removing initial condition errors in sensitive areas: A target observation perspective. *Advances in Atmospheric Sciences*, *35*(7), 853–867. <https://doi.org/10.1007/s00376-017-7138-7>
- Tao, L.-J., Zhang, R. H., & Gao, C. (2017). Initial condition error-induced optimal perturbations in ENSO predictions, as derived from an intermediate coupled model. *Advances in Atmospheric Sciences*, *34*(6), 791–803. <https://doi.org/10.1007/s00376-017-6266-4>
- Tillinger, D., & Gordon, A. L. (2009). Fifty years of the Indonesian Throughflow. *Journal of Climate*, *22*(23), 6342–6355. <https://doi.org/10.1175/2009jcli2981.1>
- Tippett, M. K., Barnston, A. G., & Li, S. (2011). Performance of recent multimodel ENSO forecasts. *Journal of Applied Meteorology and Climatology*, *51*(3), 637–654. <https://doi.org/10.1175/JAMC-D-11-093.1>
- Wang, B., Wu, R. G., & Fu, X. H. (2000). Pacific–East Asian teleconnection: How does ENSO affect east Asian climate? *Journal of Climate*, *13*(9), 1517–1536. [https://doi.org/10.1175/1520-0442\(2000\)013<1517:PEATHD>2.0.CO;2](https://doi.org/10.1175/1520-0442(2000)013<1517:PEATHD>2.0.CO;2)
- Wang, Q., Mu, M., & Dijkstra, H. A. (2013). The similarity between optimal precursor and optimally growing initial condition error in prediction of Kuroshio large meander and its application to targeted observation. *Journal of Geophysical Research: Oceans*, *118*, 869–884. <https://doi.org/10.1002/jgrc.20084>
- Webster, P. J., & Yang, S. (1992). Monsoon and ENSO: Selectively interactive systems quarterly. *Journal of the Royal Meteorological Society*, *118*(507), 877–926. <https://doi.org/10.1002/qj.49711850705>
- Wu, G. X., & Meng, W. (1998). Gearing between the Indian and Pacific Ocean (GIP) and the ENSO, Part 1. Data analyses (in Chinese). *Chinese Journal of Atmospheric Sciences*, *22*, 470–480.
- Yu, Y. S., Duan, W. S., Xu, H., & Mu, M. (2009). Dynamics of nonlinear error growth and season-dependent predictability of El Niño events in the Zebiak-Cane model quarterly. *Journal of the Royal Meteorological Society*, *135*(645), 2146–2160. <https://doi.org/10.1002/qj.526>
- Yuan, D., Wang, J., Xu, T., Xu, P., Hui, Z., Zhao, X., et al. (2011). Forcing of the Indian Ocean Dipole on the interannual variations of the tropical Pacific Ocean: Roles of the Indonesian Throughflow. *Journal of Climate*, *24*(14), 3593–3608. <https://doi.org/10.1175/2011JCLI3649.1>

- Yuan, D., Zhou, H., & Zhao, X. (2013). Interannual climate variability over the tropical Pacific Ocean induced by the Indian Ocean Dipole through the Indonesian Throughflow. *Journal of Climate*, *26*(9), 2845–2861. <https://doi.org/10.1175/JCLI-D-12-00117.1>
- Zebiak, S. E., & Cane, M. A. (1987). A model El Niño-Southern Oscillation monthly. *Weather Review*, *115*(10), 2262–2278. [https://doi.org/10.1175/1520-0493\(1987\)115<2262:ameno>2.0.co;2](https://doi.org/10.1175/1520-0493(1987)115<2262:ameno>2.0.co;2)
- Zhang, R.-H., & Gao, C. (2016). The IOCAS intermediate coupled model (IOCAS ICM) and its real-time predictions of the 2015-16 El Niño event. *Scientific Bulletin*, *61*(13), 1061–1070. <https://doi.org/10.1007/s11434-016-1064-4>
- Zhang, R.-H., Zebiak, S. E., Kleeman, R., & Keenlyside, N. (2005). Retrospective El Niño forecast using an improved intermediate coupled model. *Monthly Weather Review*, *133*(9), 2777–2802. <https://doi.org/10.1175/MWR3000.1>
- Zhou, Q., Duan, W. S., Mu, M., & Feng, R. (2015). Influence of positive and negative Indian Ocean Dipoles on ENSO via the Indonesian Throughflow: Results from sensitivity experiments. *Advances in Atmospheric Sciences*, *32*(6), 783–793. <https://doi.org/10.1007/s00376-014-4141-0>
- Zhu, J., Huang, B., Balmaseda, M., Kinter, J., Peng, P., Hu, Z.-Z., & Marx, L. (2013). Improved reliability of ENSO hindcasts with multi-ocean analyses ensemble initialization. *Climate Dynamics*, *41*(9-10), 2785–2795. <https://doi.org/10.1007/s00382-013-1965-8>